Fifth International Symposium on Marine Propulsion
smp'17, Espoo, Finland, June 2017

Hybrid Design Method for a Generic Counter-Rotating Propeller*

Emre Güngör[1]

[1]Roketsan Technology and Research Center, İstanbul, Turkey
egungor@roketsan.com.tr

ABSTRACT

In this paper, design process of a Counter-Rotating Propeller (CRP) for underwater vehicles was investigated through some hybrid approach using lifting line theory and finite volume method. Wake distribution at the inlet of front propeller surface was attained and taken into account to form the shape of profiles through blade radial. The shape of the body and CRP was generated as an unclassified configuration. Lifting line theory was performed in order to obtain pitch distribution over blades of forward and aft propellers, then the performance of CRP was observed according to Computational Fluid Dynamics (CFD) result. CRP was designed with a moderate skew and zero rake. Conventional mean-line was implemented to the geometry. Design point at rotation per minute (RPM) was required to be updated according to CFD feedback in which thrust and torque were compared against design requirements. The test-cases to represent the validation of Finite volume method was also represented in the paper by giving comparisons of torque and thrust charts of some unique propellers. Although those cases contain information about single propeller analysis and the interaction between each propeller is still crucial, they would be useful to comprehend the hybrid approach and validate the formulations inside of CFD. Reynolds Averaged Navier Stokes (RANS) and LES equations were both implemented to the finite volume method, however due to the unsteady behavior of interactions between front and aft propeller, Large Eddy Simulation (LES) formulations were commonly applied without disregarding large eddies related to mean flow quantities. On the other hand, small scales were modeled considering the fluctuations in the flow especially occurred interior domain of wake. Grid distributions around each blade was so arranged that spatial discretization should not cause to miss necessary turbulence quantities and Reynolds stresses released from leading and trailing edges. It should be noted that Sliding Mesh (SM) mechanism in which mesh is movable with respect to time was preferred due to the superiorities against Moving Reference Frame (MRF) in where the frame is frozen and the flow is rotated with a specified RPM. Time step size is also crucial that time scales should be maintained in the flow properly. The results show that hybrid method involving lifting line and finite volume method can be used as a procedure for CRP design of underwater vehicles.

Keywords

Counter-rotating propeller, design, LES, Lifting line, Finite-volume method.

1 INTRODUCTION

Counter-rotating propellers (CRP) are developed for marine vehicles to improve the efficiency of the propulsion and balance the residual moment observed on vehicle body dynamics. General perspective of design procedure and different methods was given by Carlton (2007). Design of CRP is more complicated than single propeller due to the mutual interaction between fore and aft propeller. Induced velocities generated on each blade of propeller should be taken into account to obtain a well-designed propeller however the velocity profile occurred on disc between propellers varies with time and location as a result of revolution of front propeller. Fore and aft propeller increase the velocity of flow which sweeps through the body form, therefore design process should cover effective wake on disc. A program code for CRP was generated by Caster and Lafone (1975) obtaining circulations and induced velocities on each propeller. The CRP working conditions are extremely complicated and non-uniform, however uniform conditions can give some useful information about the mechanism of CRP (Miller, 1976). Kerwin (2001) introduced single propeller design process with different methods such as lifting line, lifting surface and panel which have different characteristics to form the shape of single propeller. These techniques can be also extended to obtain wake-adapted CRP propeller giving some assumption on fore and mid-plane wake. Finite-volume method can be integrated to iterative design process in which the performance requirements are controlled and given as a feedback to the lifting line or surface method. Using of Computational Fluid Dynamics (CFD) and lifting line method might be a proper hybrid process in order to generate desired CRP geometry. Analysis of unsteady structure requires necessary knowledge on Moving Reference Frame and Sliding

Mesh technique. Unsteady Reynolds Averaged Navier Stokes (URANS) solution would give efficient time-averaged results for each time step, however due to the complicated behavior of interaction between CRP and body form, Large Eddy Simulation (LES) should be performed in numerical step. According to URANS calculations, turbulence models such as k-epsilon, k-omega etc. has to be validated via test-cases, because there is no any well-accepted unique turbulence model. In this paper, the validations were based on previous studies which are similar to current case.

The only disadvantage of lifting line and finite-volume hybrid method is time-consuming methodology while integrating both mechanisms because of the non-autonomous character while giving feedback from CFD to the lifting line. For this reason, design loop should not be higher than two or three stages in this type of hybrid structure.

2 LIFTING LINE DESIGN PROCEDURE

The in-house code in which the vortex-lattice lifting line methodology commonly based on theory represented by Kerwin (2001) was used to generate blade geometry. In this method, blade radial is divided into M segments that each segment has bound vortex strength Γ_m and free boundary vortex. For each blade, horseshoe contribution is handled in calculation. Free vortex line effects on lifting line for each control point r_c is represented by induced velocities and those were calculated by Wrench (1957). The angular speed ωr resulting from propeller revolution, tangential velocity V_t and axial velocity V_a of wake can be represented on 2D foil as illustrated in Figure 1.

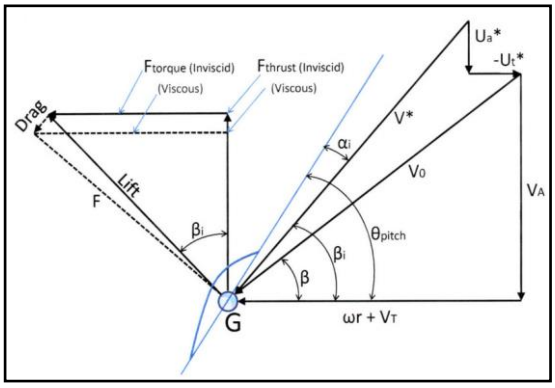

Figure 1. Velocity and angle definitions on blade profile (Epps 2010)

Each horseshoe vortex induce total axial and tangential velocities u_a^* and u_t^* on the m^{th} control point as,

$$u_a^*(m) = \sum_{i=1}^{M} \Gamma(i)\,\overline{u_a^*}(m,i) \qquad (1)$$

$$u_t^*(m) = \sum_{i=1}^{M} \Gamma(i)\,\overline{u_t^*}(m,i)$$

summed from unit vortex strength u_a^* u_t^* at i^{th} panel. The analytical description was given by Wrench (1957). In design code cosine spacing was used to determine higher resolution through blade and foil shape. The objective is to find optimum circulation with specified thrust. The flow angle β, hydrodynamic pitch angle β_i and pitch angle θ_{pitch} were given in Figure 1. Optimum circulation through blade span in algorithm was calculated according to the inputs such as vehicle speed, propeller diameter, hub geometry, design rpm and inlet wake. The flow angle β at any radius can be represented as,

$$\tan\beta(r) = \frac{V_a(r)}{\frac{\pi r}{J_s} + V_t(r)} \qquad (2)$$

then a trial value of β_i can be selected satisfying 90% of the efficiency of the actuator disk (Kerwin 2001). Circulation can be found for each β_i until desired thrust coefficient is achieved. Lerbs (1952) indicates that that kinematic relationship should be satisfied for each iteration step, therefore matrix equation for circulation can be attained as an unknown in Newton solver,

$$\sum_{m}^{M}\left[\overline{u_a^*}(n,m) - \overline{u_a^*}(n,m)\tan\beta_i(n)\right]\times\Gamma_m = \frac{V_a(n)}{V_s}\left[\frac{\tan\beta_i(n)}{\tan\beta(n)} - 1\right] \qquad (3)$$

Lastly it would be easy to form velocity triangles according to pitch angles which were optimized for each blade radial giving desired thrust. The code gives the whole propeller geometry estimating efficiency and torque at the design point. The off-design conditions were not considered in design process but CFD analysis can be used to attain all the points relating with off-design cases.

3 NUMERICAL FORMULATIONS

3.1 Flow Dynamics

The governing equations for unsteady mass and momentum conservation can be represented for constant density fluid as,

$$\frac{\partial u_i}{\partial x_i} = 0 \qquad (4)$$

$$\frac{\partial u_i}{\partial t} + u_j\frac{\partial u_i}{\partial x_j} = -\frac{1}{\rho}\frac{\partial p}{\partial x_i} + \nu\frac{\partial^2 u_i}{\partial x_j \partial x_j} \qquad (5)$$

Reynolds decomposition can be applied on (1-2) and Reynolds tensor appears in the decomposed equations below which should be handled using some turbulence models,

* Leave blank the last 2.0 cm on the first page to place some additional informational about this paper in a footnote on the first page if necessary.

$$\frac{\partial \bar{u}_i}{\partial x_i} = 0 \tag{6}$$

$$\frac{\partial u_i}{\partial t} + u_j \frac{\partial u_i}{\partial x_j} = -\frac{1}{\rho}\frac{\partial p}{\partial x_i} + \nu \frac{\partial^2 u_i}{\partial x_j \partial x_j} \tag{7}$$

Turbulent kinetic energy (TKE) can be defined by,

$$\frac{\partial(\rho k)}{\partial t} + \frac{\partial(k u_i)}{\partial x_i} = \frac{\partial}{\partial x_i}\left[\left(\alpha_k \mu_{eff}\right)\frac{\partial k}{\partial x_i}\right] + G_k + G_b - \rho\varepsilon - Y_M \tag{8}$$

where k and ε denote turbulent kinetic energy and the rate of dissipation, respectively. The term G_k represents the turbulent kinetic energy production due to the change of velocity in space, G_b is the turbulent kinetic energy production due to the buoyancy forces and Y_M is the contribution of the fluctuating dilatation in compressible turbulence which is zero for the present case. The rate of dissipation can be defined by,

$$\rho\frac{D\varepsilon}{Dt} = \frac{\partial}{\partial x_j}\left[\left(\mu + \frac{\mu_t}{\sigma_\varepsilon}\right)\frac{\partial \varepsilon}{\partial x_j}\right] + C_{1\varepsilon}\frac{\varepsilon}{k}\left(G_k + C_{3\varepsilon}G_b\right) - C_{2\varepsilon}\rho\frac{\varepsilon^2}{k} \tag{9}$$

RNG model is used due to its response to the influences of rapid strain and streamline curvature than standard k-ε (Ansys 2010).

On the other hand, the Large Eddy Simulation (LES) formulation, which low pass filters the solution in which smallest scales are modeled and large scales are resolved, was used to capture the unsteady fluctuations and so to determine the detailed behavior of the flow field. Prior to this study, URANS and LES formulations were both examined, however due to the acoustical approach which will be considered in future studies LES was decided for flow calculations. Because in order to satisfy the Courant–Friedrichs–Lewy (CFL) condition (Blazek 2001) and minimum element per wavelength criteria (Howard ve Cazzolato 2015) it requires very small time steps and element size to be used. Element size and time step was selected observing the minimum wavelength and Nyquist criteria.

3.1.1 LES Calculations

Large scale motions are much more energetic than small scale ones. Therefore they can be easily used to describe flow characteristics. On the other hand large scale simulations are expensive, time dependent and three dimensional. In order to attain velocity field containing large scales, we need a filtering mechanism in flow field. Local average of the complete field results in resolved scale field that one to be simulated (Ferziger and Peric, 2002). Filtered velocity is defined as,

$$\bar{u}_i(x) = \int G(x, x')u_i(x')dx' \tag{10}$$

In this equation G(x,x') is the filter kernel consisting local average and cutoff region. Eddies larger than filter length scale are large eddies that need to be solved. However smaller eddies should be modeled according to filtering. When incompressible flow is filtered, a set of equations can be attained both for momentum and mass.

$$\frac{\partial \rho\bar{u}_i}{\partial t} + \frac{\partial\left(\rho\overline{u_i u_j}\right)}{\partial x_i} = -\frac{\partial \bar{p}}{\partial x_j} + \frac{\partial}{\partial x_j}\left[\mu\left(\frac{\partial \bar{u}_i}{\partial x_j} + \frac{\partial \bar{u}_j}{\partial x_i}\right)\right] \tag{11}$$

$$\frac{\partial \rho\bar{u}_i}{\partial x_i} = 0 \tag{12}$$

Subgrid-scale Reynolds Stress can be shown as,

$$\tau_{ij}^s = -\rho\left[\left(\overline{\rho u_i u_j}\right) - \bar{u}_i\bar{u}_j\right] \tag{13}$$

and it refers to the large scale momentum flux caused by action of small scales which has to be modeled. Smagorinsky proposed a model as,

$$\tau_{ij}^s - \frac{1}{3}\tau_{ij}^s\delta_{ij} = \mu_t\left(\frac{\partial \bar{u}_i}{\partial x_j} + \frac{\partial \bar{u}_j}{\partial x_i}\right) \tag{14}$$

In this equation right hand side contains strain rate of large scale and eddy viscosity.

3.2 Flow Solver

The transport equations were solved using finite volume method with a pressure-based solver which utilizes the integral formulation of the Navier Stokes equations (Blazek 2001). Therefore, the physical domain was divided in a mesh structure consisting of small tetrahedral cells, where the spatial discretization scheme was very important. The other critical issues were the temporal discretization and the selection of the turbulence model. A second order discretization scheme was chosen for the convective and viscous terms of the governing equations. The propeller blades were exposed to the inflow which evolved in time due to the nonhomogeneous wake. The sliding mesh technique (Ansys 2010) was used to represent the rotation in which the interfaces of the propeller domain were rotated with a time step optimized before the calculations. The pressure segregated algorithm iterated the solution until the convergence was satisfied. ANSYS® were used to solve flow dynamics.

4 CFD CALCULATIONS AND PROPELLER DESIGN

The vehicle body selected as an unclassified type was supposed to be propelled by CRP which rotates with a specific design RPM (revolution per minute). Inputs to the propeller design should be coupled with operating conditions and results of CFD calculations. Operating conditions were assumed as,

Table 1. Operating conditions

Property	Symbol	Value
Vehicle speed	*V*	15.42 m/s
Operating depth	*H*	50 m
Water density	P	1020 kg/m^3
Fore propeller RPM	n_f	1000
Aft propeller RPM	n_a	1000

The vehicle geometry has a generic body cap and rudder/elevator as given in Figure 2. The main geometry dimensions were listed in Table 2.

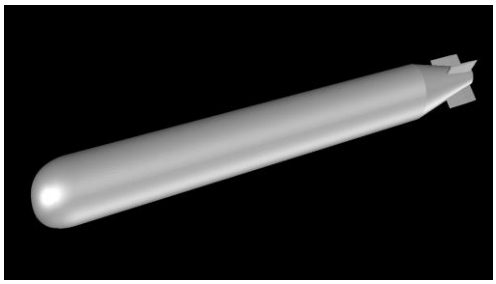

Figure 2. Generic (unclassified) underwater vehicle body

Table 2. Body Main Dimensions

Property	Symbol	Value
Vehicle length without CRP	*L*	4984 mm
Diameter	*D*	426 mm
Aft diameter	d	141 mm
Rudder number	-	2
Elevator number	-	2

CFD calculation was applied on the body to attain wake in front of forward propeller and to find whole body drag as an input for CRP design.

4.1 Flow Dynamics on Body

In order to achieve proper results from CFD, discretization, mesh dependency and turbulence model should be validated against some test-cases. These detailed comparisons were performed in previous studies and proper model has been already decided according to Güngör and Özdemir (2015). RANS equations were solved at each time-step while attaining drag and wake around body without CRP. However Unsteady RANS and LES should be applied because of the nonhomogeneous behavior and complicated interaction between fore and aft propeller. Mesh dependency was also observed in different cases. In order to have high accuracy local and time was discretized with second order formulation. The flow was constant over time thus steady calculations are valid in this case except rotating conditions. The unstructured fine mesh was illustrated in Figure 3.

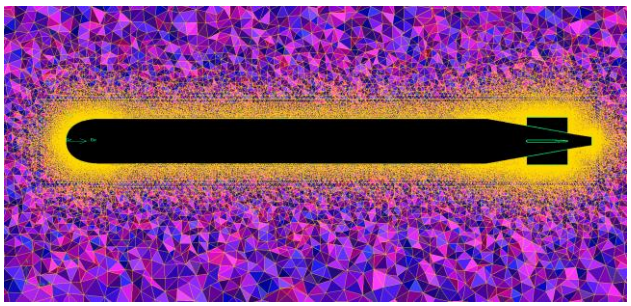

Figure 3. Fine mesh generated in flow volume

The details about the solution step were given in Table 3.

Table 3. Preparations for Body Analysis without CRP

Property	Specification
Flow speed	15.42 m/s
Mesh cell size	7.8 millions
Boundary layer number	6
y+	Max. 2.75
Inlet Boundary Condition	Const. Velocity
Outlet Boundary Condition	Const. Pressure
Mesh type	Unstructured tetra.
Turbulence model	k-epsilon RNG
Solver type	Pressure based RANS
Spatial discretization	2nd order

4.1.1 Mesh Dependency Study wrt. Drag

Before Coarse, medium and fine mesh size was compared against each other to isolate mesh dependency factor. Coarse, medium and fine mesh has 5.34, 7.8, 8.1 million cells respectively. Figure 4 shows that medium mesh is well accepted model to perform further numerical calculations, because higher mesh size results in much longer solution time.

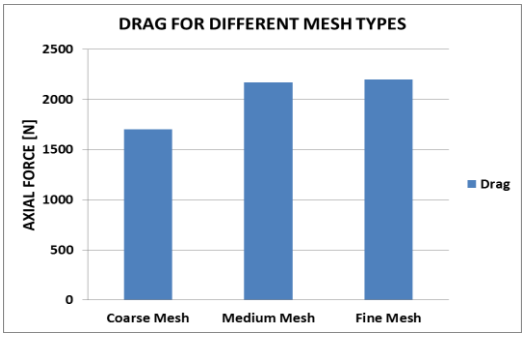

Figure 4. Mesh model comparison

4.1.2 Nominal Wake

Boundary layer was so arranged that y+ value lower than 3.5 was achieved around body (Figure 5). Simulations were run on PC with 16 processors and 256 GB RAM for approximately 8 hours until residuals dropped down iteratively lower than 10E-5. As a result, force on the rudder plane and elevator plane was negligible due to symmetry conditions, however axial force was calculated as a drag input for CRP design. In Figure 6 nominal wake on the front plane of forward propeller and circumferentially distributed circles to calculate averaged nominal wake through blade radial can be seen.

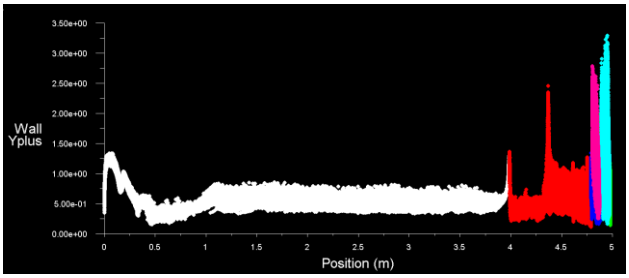

Figure 5. Boundary layer y+ value through axial position

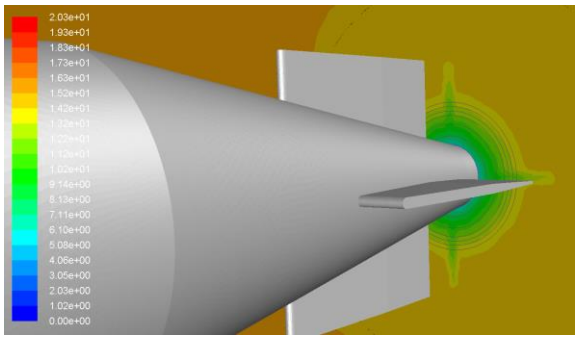

Figure 6. Nominal wake plotted on CRP inlet plane

This nominal wake was normalized and homogenized for each radial passage to place wake information at proper locations in CRP design.

4.2 CRP Design Step (Phase 1)

The assumed main geometry for the forward and aft propeller can be seen in Table 4.

Table 4. CRP Main Dimensions

Property	Fore Prop	Aft Prop
Hub diameter	125 mm	95 mm
Tip Diameter	344 mm	336 mm
Hub length	95	95 mm
Design rpm	1000	1000
Blade number	7	5

Initially nominal wake, geometry details and thrust deduction coefficient (assumed as %20), body drag with

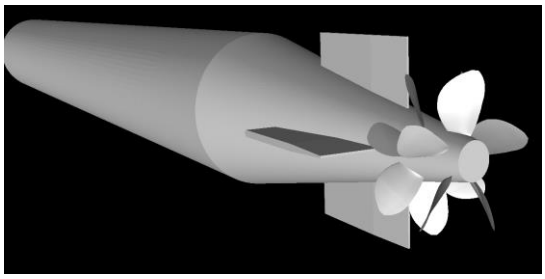

Figure 7. CRP Geometry from back-view

appendages and desired thrust were all fed into the design algorithm which produce hydrofoil profile section for each segment along blade. Thickness, camber, skew and chord details were so arranged that meaningful generic shape could be achieved. After fore propeller was designed according to requirements, aft propeller geometry was attained in code regarding to wake from fore propeller. Due to the rotation of propeller, the flow speed was increased in axial direction therefore propeller design speed would be higher than vehicle current speed. Total desired thrust was equally distributed to both propeller (approx. 1375 N at 15.42 m/sn and 1000 rpm)

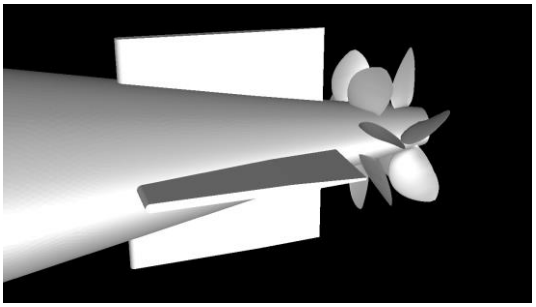

Figure 8. CRP Geometry from side-view

5 PERFORMANCE ANALYSIS AND CFD FEEDBACK

When the design process was finished, propeller performance was observed with CFD calculations. Rotation effect and interactions require Sliding Mesh (SM) technique and unsteady solutions. URANS and LES were both applied to the system and performance was observed until convergence criteria were satisfied.

5.1 RANS Steady Solutions

Although unsteady behavior dominates the flow characteristics, convergence would be much easier by starting with RANS steady calculation. Table 5 gives results representing propeller performance and body drag resulted from propeller rotation.

Table 5. RANS Steady CFD results

Property	Value
Body drag with prop.	2867 N
Fore Thrust	805 N
Aft Thrust	1756 N
Fore Moment	125 Nm
Aft Moment	251 Nm
Body Moment	3.9 Nm

In design step, it was aimed that thrust was equally distributed to both propeller and moment was not restricted. However performance analysis showed that fore propeller does not exhibit requirement, therefore URANS calculations should be performed to make sure that design point was shifted from optimum case.

5.2 URANS Sliding Mesh Solutions

In this technique, propeller volume mesh rotates with a time step size defined preliminarily with respect to outer domain and convergence should be ensured at each iteration. Time step size (1.6E-04) was selected regarding to the blade passing frequency. Actuators interrupts the homogenous inflow to CRP, thus interruption effect was taken place in spectrum domain while post-processing the results. Table 6 shows results obtained in URANS SM.

Table 6. URANS SM results

Property	Value
Body drag with prop.	2980 N
Fore Thrust	755 N
Aft Thrust	1763 N
Fore Moment	120 Nm
Aft Moment	253 Nm
Body Moment	1.8 Nm

Thrust fluctuations were stored at each time step and after nine whole rotations they were plotted as in Figure 9. The convergence tendency can be seen in time domain.

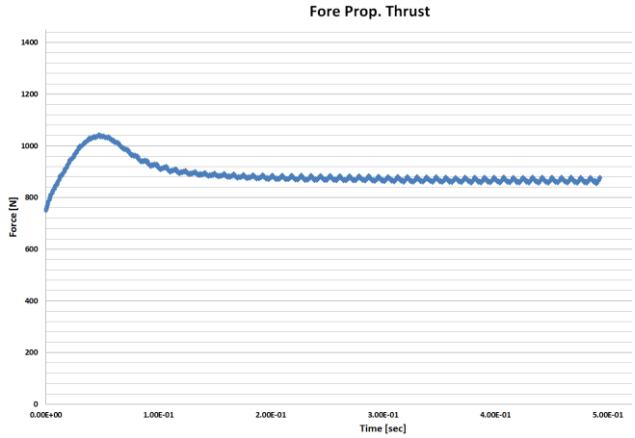

Figure 9. Fore Propeller Thrust fluctuations in time

The data contains much information in frequency domain such as actuators interruption, blades interference and mutual interaction between propellers. This is shown in Figure 10.

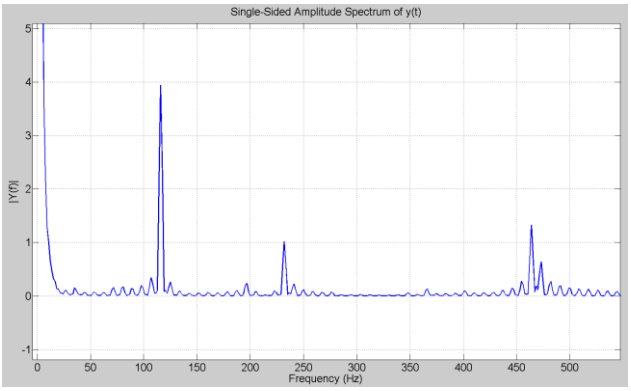

Figure 10. Single-sided Amplitude Spectrum of Fore Thrust

Single-sided spectrum illustrates blade passing frequency, its harmonics and the vortex shedding from each blade in time.

5.2 LES Sliding Mesh Solutions

For further applications dealing with spectral solutions, LES formulation was used to capture the unsteady fluctuations and so to determine the detailed behavior of the flow field. In this simulation smallest scales are modeled and large scales are resolved, therefore flow structures can be more easily represented than time-averaged Navier-Stokes calculations as shown in contour plot of vorticity (Figure 11).

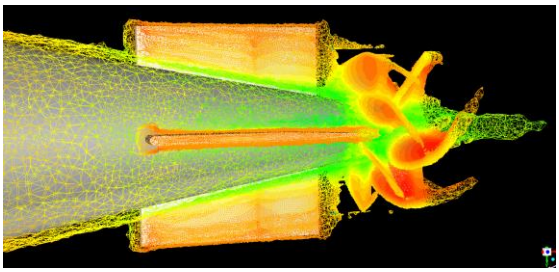

Figure 11. Vorticity distribution (around 200 1/s) shedding from appandages and blades into the flow domain

These data can be used to couple with acoustical calculations or vibration analysis as a further study. LES computations are much more sophisticated and detailed than URANS calculations that small scales are clearly apparent in Figure 12. Small structures can be easily handled by using LES instead of URANS due to the resolving of large eddies and modeling the small ones.

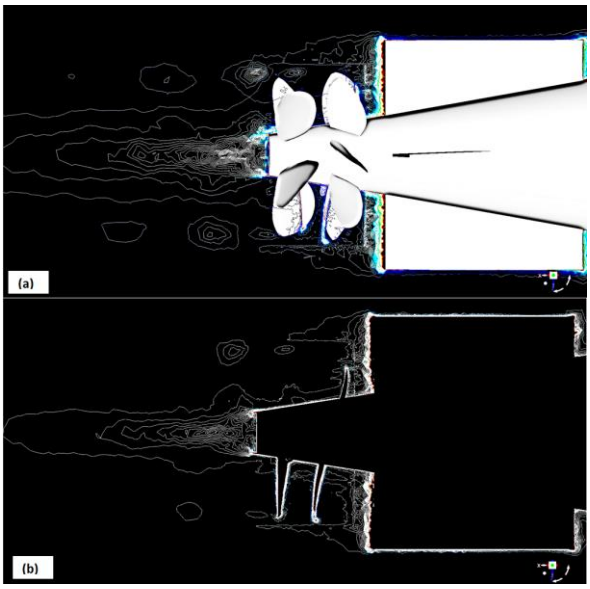

Figure 12. Vorticity (around 3000 1/s) distribution after using a) LES and b) URANS

6 CRP 1st MODIFICATION PHASE

Because of the mismatch for desired thrust, forward propeller requires a modification with the aid of CFD feedback. At the design stage, disregarding of aft propeller effect on the inflow speed towards fore propeller could be the reason for mismatching. Therefore pitch modification can avoid getting lower performance at forward propeller. Due to the lower thrust pitch should be increased iteratively, however lifting line and finite volume hybrid method does not allow so many iteration steps. The performance table was attained after initial pitch value was increased by 5 percent and steady analysis was performed on the modified propeller (Table 7). As shown in Figure 13, pitch correction can be comprised by initial model.

Table 7. RANS Steady CFD results after 1st modification

Property	Value
Body drag with prop.	2840 N
Fore Thrust	995 N
Aft Thrust	1570 N
Fore Moment	150 Nm
Aft Moment	230 Nm
Body Moment	3 Nm

Fore propeller thrust was increased due to the pitch modification and aft propeller thrust was decreased because of the increase in forward blade leading edge angle. However design point was not achieved sufficiently and new design should be given to CRP system.

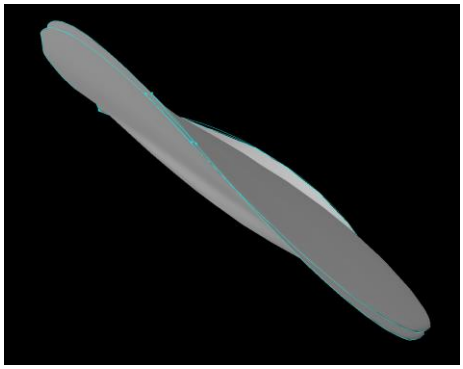

Figure 13. Forward blade pitch correction by 5 percent (view from blade top)

7 CRP 2nd MODIFICATION PHASE

The final modification was based on forward pitch increase by 15 percent (Figure 14) and this modification resulted in achievement of desired thrust as shown in Table 8. Aft propeller performance was converged in design point without losing its efficiency.

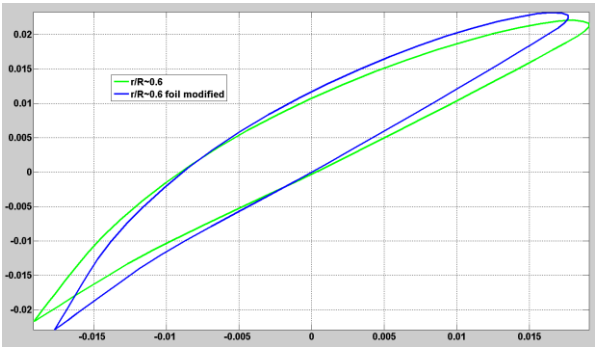

Figure 14. Forward blade pitch correction by 15 percent

Table 8. RANS Steady CFD results after 2st modification

Property	Value
Body drag with prop.	2910 N
Fore Thrust	1390 N
Aft Thrust	1450 N
Fore Moment	170 Nm
Aft Moment	200 Nm
Body Moment	3.2 Nm

It should be noted that performance was not expected to be perfectly matched with design point. Therefore this tolerance was assumed enough for underwater vehicle requirements. The modification phase was finished having optimum design for underwater vehicle speed and wake. Steady RANS calculations were considered to be fast prediction method under some assumptions. Time-accurate variations on thrust or torque could not be attained by this type of steady solutions; however initial CFD analysis showed that time-averaged solutions were nicely represented by steady cases extremely much faster than unsteady methods.

7 CONCLUSION

In this paper CRP design was performed using hybrid approach for known generic underwater vehicle geometry. Wake adapted propeller was design using lifting line method and its result was coupled with a finite-volume CFD solver. RANS, URANS and LES calculations were both compared each other in order to see the differences in thrust, torque, body drag. LES with a sliding mesh technique results give better spectral information; on the other hand RANS calculations were extremely faster than other solvers. CFD analysis showed that steady solutions can be used to compare each blade design but performance had to be observed in unsteady case more accurately. Three design step was required to attain desired performance regarding to CFD feedback. Due to the lack of fast setup module, it would not be easy to implement modified blade design to the process, therefore iteration was limited to three. In this study, cavitation and acoustical approach was not taken into account. In future, blade design can be modified considering cavitation effect or acoustical requirement. Acoustic sources from CFD can be coupled with Finite Element Modelling or Boundary Element Modeling to generate blade geometry correcting not only pitch but also skew and thickness distribution.

REFERENCES

Carlton, J. (2007). Marine Propellers and Propulsion, Elsevier.

Caster, E. B., LaFone, T. A. (1975). 'A computer Program for the Preliminary Design of Contrarotating Propellers'. David W. Taylor Naval Ship Research and Development Center.

Kerwin, J. E. (2001). Lecture Notes: Hydrofoils and Propellers. MIT.

Miller, M. L. (1976). 'Experimental Determination of Unsteady Forces on Contrarotating Propellers in Uniform Flow'. David W. Taylor Naval Ship Research and Development Center.

Wrench, J.W. (1957). 'The calculation of propellers induction factors'. DTMB Report 1116.

Laskos, D. (2010). ‘Design and cavitation performance of contra-rotating propellers’. MIT.

Epps, B. (2010). OpenProp v2.3 - Theory document. MIT.

Lerbs, H.W. (1952). ‘Moderately loaded propellers with finite number of blades and an arbitrary distribution of circulation’. SNAME, Vol.60.

Ansys (2010). Ansys v13 Fluent User's Guide. USA.

Blazek, J. (2001). Computational Fluid Dynamics: Principles and Applications. Switzerland: Elsevier.

Howard, C. Q., Cazzolato, S. (2015). Acoustic Analyses Using MATLAB and ANSYS. CRC Press Taylor & Francis Group.

Güngör, E. and Özdemir, I. B. (2015). ‘Design and analyses of a propeller for underwater vehicles using computational fluid dynamics’. Proceedings of the 6th InternationalConference on Mechanical and Aerospace Engineering (ICCMAE), 16–17 July, Rome, Italy.

Ferziger, J. H., Peric, M. (2002). Computational Methods for Flow Dynamics. Springer-Verlag, Berlin Heidelberg.